Bioinspired optofluidic FRET lasers via DNA scaffolds

Yuze Sun[a,b], Siyka I. Shopova[b,c], Chung-Shieh Wu[b], Stephen Arnold[c], and Xudong Fan[a,b,1]

[a]Biomedical Engineering Department, University of Michigan, 1101 Beal Avenue, Ann Arbor, MI 48109; [b]Department of Biological Engineering, Bond Life Sciences Center, University of Missouri, Columbia, MO 65211; and [c]MicroParticle PhotoPhysics Lab, Polytechnic Institute of New York University, Brooklyn, NY 11201

Edited by Federico Capasso, Harvard University, Cambridge, MA, and approved July 22, 2010 (received for review March 17, 2010)

Optofluidic dye lasers hold great promise for adaptive photonic devices, compact and wavelength-tunable light sources, and micro total analysis systems. To date, however, nearly all those lasers are directly excited by tuning the pump laser into the gain medium absorption band. Here we demonstrate bioinspired optofluidic dye lasers excited by FRET, in which the donor-acceptor distance, ratio, and spatial configuration can be precisely controlled by DNA scaffolds. The characteristics of the FRET lasers such as spectrum, threshold, and energy conversion efficiency are reported. Through DNA scaffolds, nearly 100% energy transfer can be maintained regardless of the donor and acceptor concentration. As a result, efficient FRET lasing is achieved at an unusually low acceptor concentration of micromolar, over 1,000 times lower than that in conventional optofluidic dye lasers. The lasing threshold is on the order of $\mu J/mm^2$. Various DNA scaffold FRET lasers are demonstrated to illustrate vast possibilities in optofluidic laser designs. Our work opens a door to many researches and applications such as intracavity bio/chemical sensing, biocontrolled photonic devices, and biophysics.

fluorescence resonance energy transfer | optofluidics | ring resonators

Optofluidic lasers are an emerging technology that combines the advantages of compactness and easy liquid manipulation of microfluidics, and dynamic wavelength tunability and broad spectral coverage of dye lasers (1–3). Optical feedback in those optofluidic lasers has been achieved using high-Q ring resonators [e.g., microdroplets (4, 5), microspheres (6), microcylinders (7), microcapillaries (8, 9), and microfiber knots (10)], Fabry-Pérot cavities (11, 12), and distributed feedback gratings (3, 13). In nearly all those lasers, the gain medium is directly excited by tuning the pump laser into the dye absorption band, which requires that the pump laser wavelength match the particular dye absorption. An alternative excitation scheme is through energy transfer, in which dye mixtures, composed of the donor and the acceptor, are used. Donors are directly excited and subsequently transfer energy to acceptors for lasing. The energy transfer significantly extends the laser emission wavelength range without the need to change the pump wavelength. Moreover, dye lasers based on energy transfer have a much higher pump efficiency and lower lasing threshold than the corresponding single dye lasers due to the low donor absorption loss at the acceptor lasing wavelength (14, 15).

Generally, there are two transfer mechanisms between the donor and the acceptor in an optical cavity: nonradiative FRET (14–17), in which the transfer is mediated by short-ranged resonant dipole–dipole interaction, and cavity-assisted radiative transfer (18–20), in which the emission from the donor is first coupled into the cavity, which stores photons for an extended amount of time before they are reabsorbed by the acceptor. The FRET efficiency between a donor and acceptor pair is $R_0{}^6/(R_0{}^6+r^6)$, where R_0 and r are the Förster distance and the donor–acceptor distance, respectively. The cavity-assisted transfer efficiency is determined by the fraction of donor emission into cavity modes and the probability of acceptor reabsorption (18, 19) (see *SI Text* for detailed analysis). Unfortunately, to date only a handful of energy transfer based optofluidic lasers have been demonstrated (15, 17). In those lasers, the donor and the acceptor are distributed homogeneously in solution. Therefore, the transfer efficiency can be determined only by the donor and acceptor concentrations (i.e., the averaged donor–acceptor distance), which diminishes rapidly at decreased donor and acceptor concentrations. Additionally, although vastly different, the respective contribution of FRET and the cavity-assisted energy transfer in optofluidic lasers has not been well elucidated (17), due in part to the lack of an approach to precisely control the donor–acceptor distance in the gain medium. How to better understand and control the energy transfer processes and how to maintain high transfer efficiency at low donor and acceptor concentrations are particularly important for the development of optofluidic lasers, and for their applications in bio/chemical sensing and biophysics.

Here we investigate bioinspired optofluidic dye lasers utilizing FRET via DNA scaffolds (see Fig. 1), in which the donor and acceptor are conjugated with DNA sequences with the predetermined donor-to-acceptor distance, ratio, and spatial configuration (21–25). Because the donor and the acceptor are maintained within the Förster distance by DNA scaffolds, high energy transfer efficiency can be obtained regardless of the donor and acceptor concentrations. As a result, we are able to achieve efficient FRET lasing even with an acceptor concentration as low as 2.5 μM. Various DNA scaffolds are demonstrated to exemplify vast possibilities in optofluidic laser designs.

The FRET lasers are performed using the optofluidic ring resonator (OFRR) (9, 15), a thin-walled fused silica capillary that integrates the high-Q-factor ring resonator with microfluidics. As illustrated in Fig. 1, the capillary cross-section forms a ring resonator and the whispering gallery modes (WGMs) interact evanescently with the dye solution flowing through the OFRR. The fabrication of the OFRR and the microfluidic laser-related experimental setup can be found in *Materials and Methods*.

Results and Discussion

A simple OFRR FRET laser can be achieved through a one-donor-one-acceptor (1D1A) scaffold by using complementary ssDNAs, 1D1A-Cy3 and 1D1A-Cy5, with the donor (Cy3) and the acceptor (Cy5) conjugated to the 3′ end of each ssDNA (see *Materials and Methods*, Tables S1 and S2, and Fig. S1 for details of DNA samples used in experiments). During the experiment the excitation laser wavelength is 518.3 nm, which is within the donor absorption band (see Fig. S1). Fig. 2*A* shows the lasing emission spectrum after DNA hybridization at a concentration of 30 μM for both donor and acceptor. A number of quasiperiodic lasing peaks emerge around 720 nm first. With the increased pump intensity, this group of lasing emission gradually levels off and meanwhile the lasing emission at shorter wavelengths (around 690 nm) starts to occur, as expected (7). Both wavelength

Author contributions: Y.S. and X.F. designed research; Y.S. performed research; Y.S., S.I.S., C.-S.W., S.A., and X.F. analyzed data; and Y.S., S.I.S., S.A., and X.F. wrote the paper.

The authors declare no conflict of interest.

This article is a PNAS Direct Submission.

[1]To whom correspondence should be addressed. E-mail: xsfan@umich.edu.

This article contains supporting information online at www.pnas.org/lookup/suppl/doi:10.1073/pnas.1003581107/-/DCSupplemental.

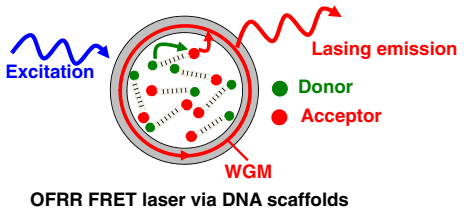

Fig. 1. Conceptual illustration of OFRR FRET lasers via DNA scaffolds. The donor transfers energy to the acceptor through FRET that is precisely controlled by DNA scaffolds. Note that the donor and the acceptor are labeled on complementary ssDNAs. WGM, whispering gallery mode.

ranges are within the Cy5 emission band. No lasing emission is observed for Cy3 in the wavelength range of 570–650 nm, i.e., the Cy3 emission band. As a negative control, we perform the same experiment with 30 μM of 1D1A-Cy5 alone (Fig. S2*a*). No lasing emission from Cy5 is observed when pumped at 518.3 nm, suggesting that Cy5 cannot be directly excited to achieve lasing at this pump wavelength and that the lasing emission from Cy5 in Fig. 2*A* indeed result from the energy transferred from Cy3. Fig. 2*B* plots the total laser emission around 690 nm and around 720 nm as a function of the pump energy density. The respective lasing threshold is 6.8 $\mu J/mm^2$ and 4.2 $\mu J/mm^2$.

An additional control experiment presented in Fig. S2*b* allows us to distinguish the two energy transfer mechanisms from one another. In this experiment, Cy3 lasing occurs when 30 μM of 1D1A-Cy3 sample alone is pumped under exactly the same conditions as in Fig. 2*A*. However, when 1D1A-Cy5 is added, the Cy3 lasing is quenched with the concomitant appearance of Cy5 lasing emission (see Fig. 2*A*), suggesting that the nonradiative FRET plays a dominant role in energy transfer (17, 26) (more control experiments and discussion can be found in *SI Text*). Through a DNA scaffold, the distance between Cy3 and Cy5 and hence the FRET efficiency can be determined by the hybridized DNA length. Given the Förster distance for Cy3 and Cy5 of 6 nm (see Table S2) and the Cy3-Cy5 distance of 4.08 nm (assuming 0.34 nm per DNA base pair), the FRET efficiency from Cy3 to Cy5 is calculated to be 91%.

The OFRR laser can be controlled not only by the donor–acceptor distance, but also by the DNA scaffold that changes the donor-to-acceptor ratio. With the increased donor-to-acceptor ratio, more pump energy can be absorbed by the laser system, resulting in a lower lasing threshold and a higher pump efficiency (14). As illustrated in the inset of Fig. 3*A*, we construct a DNA scaffold consisting of two-donor-one-acceptor (2D1A) by self-assembly of three ssDNAs. In this 2D1A system, the donor (Cy3) is attached to the 3′ and 5′ end of a ssDNA sequence, respectively [2D1A-Cy3(3′) and 2D1A-Cy3(5′); see Table S1]. The acceptor (Cy5) is labeled on the adenine base in the middle of the ssDNA sequence (2D1A-Cy5), which serves as a DNA backbone for hybridization with 2D1A-Cy3(3′) and 2D1A-Cy3(5′).

After hybridization, the distance between each Cy3 and Cy5 pair is 4.08 nm, the same as that in the 1D1A case discussed previously. Thus the donor-to-acceptor ratio is doubled, whereas the donor–acceptor distance remains unchanged. The corre-

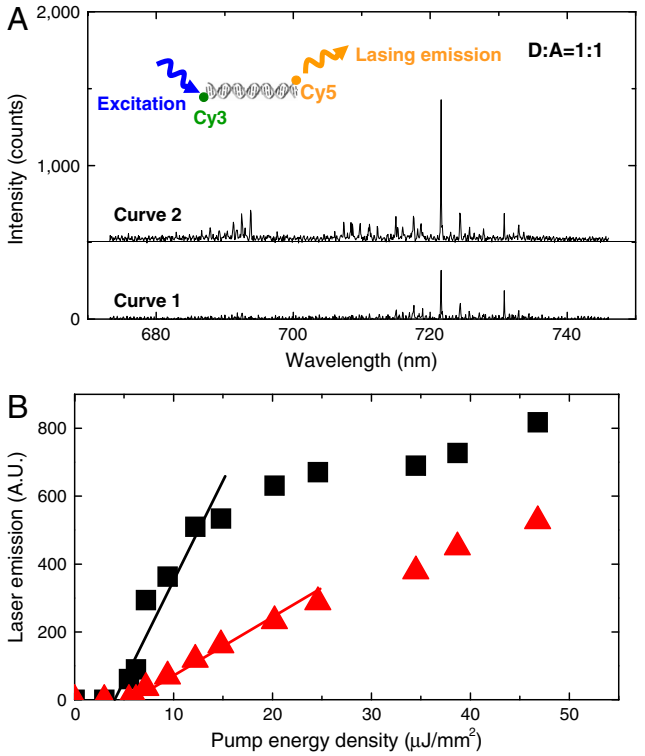

Fig. 2. (*A*) OFRR FRET lasing emission spectra for the donor-to-acceptor ratio of 1:1 achieved through hybridization of 1D1A-Cy3 and 1D1A-Cy5. The concentration of both ssDNA samples is 30 μM. Laser excitation wavelength is 518.3 nm. Curves 1 and 2 are the spectrum slightly and well above the lasing threshold, respectively. Curves are vertically shifted for clarity. (*Inset*) The corresponding DNA scaffolds. (*B*) Laser emission as a function of pump energy density per pulse. Triangles, laser emission integrated between 680 nm and 700 nm; squares, laser emission integrated between 700 nm and 740 nm. Solid curves are the linear fit of the linear part of the integrated laser emission. Lasing threshold is 6.8 $\mu J/mm^2$ and 4.2 $\mu J/mm^2$ for the laser emission centered at 690 nm and 720 nm, respectively.

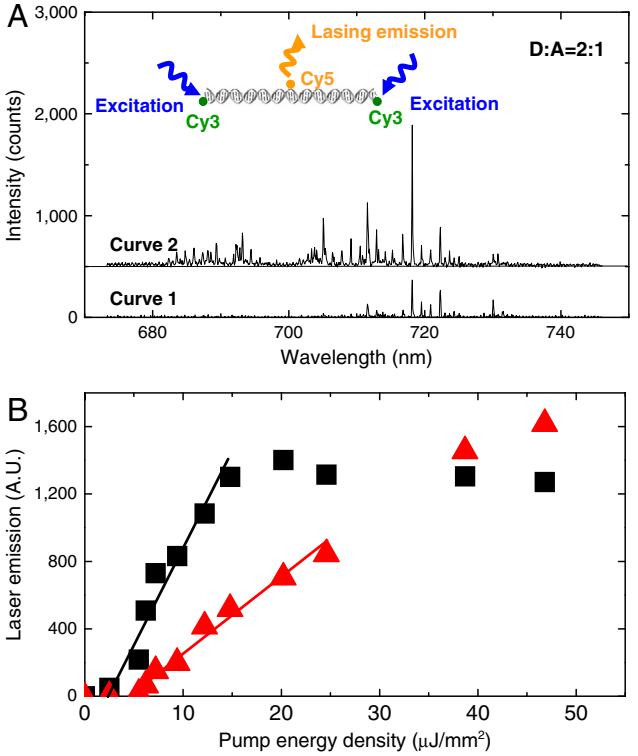

Fig. 3. (*A*) OFRR FRET lasing emission spectrum for the donor-to-acceptor ratio of 2:1 achieved through hybridization of 2D1A-Cy3(3′), 2D1A-Cy3(5′), and 2D1A-Cy5. The concentration of all ssDNA samples is 30 μM. Laser excitation wavelength is 518.3 nm. Curves 1 and 2 are the spectrum slightly and well above the lasing threshold, respectively. Curves are vertically shifted for clarity. (*Inset*) The corresponding DNA scaffolds. (*B*) Laser emission as a function of pump energy density per pulse. Triangles, laser emission integrated between 680 nm and 700 nm; squares, laser emission integrated between 700 nm and 740 nm. Solid curves are the linear fit of the linear part of the integrated laser emission. Lasing threshold is 4.4 $\mu J/mm^2$ and 2.3 $\mu J/mm^2$ for the laser emission centered at 690 nm and 720 nm, respectively.

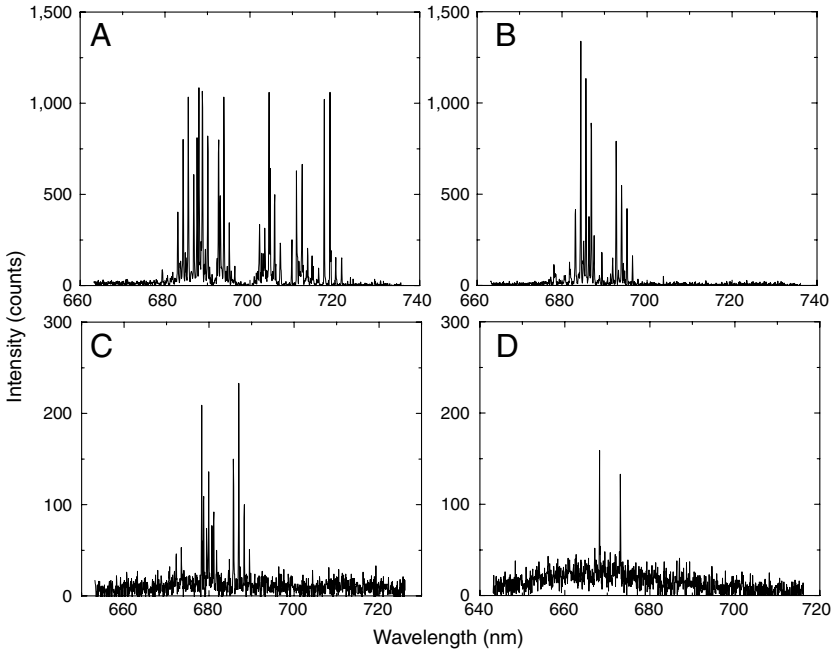

Fig. 4. Emission spectrum of 2-donor-1-acceptor FRET lasers at various ssDNA concentrations. (*A*) 30 μM, (*B*) 15 μM, (*C*) 5 μM, and (*D*) 2.5 μM. The pump energy density per pulse is fixed at 54 μJ/mm^2.

sponding lasing emission spectrum is present in Fig. 3*A*, which has quasiperiodic lasing peaks similar to Fig. 2*A*. At the same pump intensity, the FRET lasing intensity in the 2D1A system is stronger than that in the 1D1A system and more lasing peaks emerge. The corresponding lasing threshold curve in Fig. 3*B* shows a lasing threshold of approximately 4.4 μJ/mm^2 and 2.3 μJ/mm^2 for the laser emission centered at 690 nm and 720 nm, respectively, which are approximately half of their corresponding threshold for the 1D1A system. Additionally, the lasing differential efficiency, i.e., the slope of the curve in Fig. 3, is nearly doubled in the 2D1A system in comparison with the 1D1A system for both 690 nm and 720 nm bands.

As discussed earlier, through a DNA scaffold the high energy-transfer efficiency can be maintained regardless of the donor or acceptor concentration. In Fig. 4, we explore the minimum gain medium concentration that can achieve lasing via FRET using 2D1A samples of 30 μM, 15 μM, 5 μM, and 2.5 μM, respectively. It is shown that the laser emission persists even at an unprecedented concentration of 2.5 μM with a lasing threshold well below 50 μJ/mm^2, nearly 1,000 times lower than the dye concentration used in other types of optofluidic lasers. Considering that the WGM interacts with only a few picoliters of dye solution near the OFRR inner surface, the total number of dye molecules contributing to the laser emission is estimated to be on the order of 10^7.

The same DNA scaffold design principles can further be applied to develop cascade FRET lasers to extend the lasing emission wavelength range. Similar to the 2D1A structure, we now hybridize three ssDNA sequences, Cascade-Cy3, Cascade-Cy5, and Cascade-Cy5.5 (see Table S1). After hybridization, the distance from Cy3 to Cy5 and from Cy5 to Cy5.5 is 4.42 nm, corresponding to a transfer efficiency of 86% (Cy3-Cy5), 95% (Cy5-Cy5.5), and 8% (Cy3-Cy5.5), respectively. Therefore, the majority of energy is transferred from Cy3 to Cy5.5 via Cy5. Cascade FRET lasing emission from Cy5.5 is shown in Fig. 5*A* at the pump wavelength of 518.3 nm. No lasing emission is observed from Cy3 or Cy5. Control experiments (see Fig. S3) confirm that Cy5 and Cy5.5 cannot be directly excited to achieve lasing at this pump wavelength. Lasing threshold in Fig. 5*B* is measured to be approximately 6 μJ/mm^2.

Note that the cavity-assisted energy transfer may also play a role in supporting the acceptor lasing. The experimental results and theoretical analysis of the contribution from the cavity-assisted energy transfer can be found in the discussion associated with Figs. S4–S7.

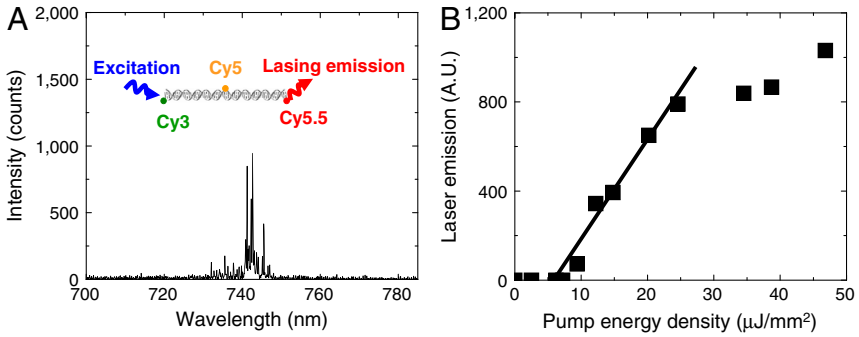

Fig. 5. Cascade OFRR FRET laser. (*A*) Lasing emission spectrum. Laser excitation wavelength is 518.3 nm. The concentration of all ssDNAs is 30 μM. (*Inset*) The DNA scaffold structure that bridges Cy3, Cy5, and Cy5.5. (*B*) Lasing emission integrated between 720 nm and 760 nm versus pump energy density per pulse. Solid curve is the linear fit of the linear part of the integrated laser emission. Lasing threshold is 6 μJ/mm^2.

Conclusions

We have demonstrated the FRET-based optofluidic dye laser via various DNA scaffolds, through which FRET is a dominant energy transfer mechanism and high transfer efficiency can be maintained in an extremely large concentration range (from a single donor/acceptor pair up to approximately 1 mM). FRET lasing at 2.5 μM has been achieved. With further improvement in the excitation scheme (e.g., tapered fiber excitation at a WGM resonant wavelength), Q factors, and DNA scaffold designs, and using donors with larger absorption cross-sections [such as quantum dots (15) and DNA binding fluorescent conjugated polymers (27)], lasing at nanomolar range is possible.

We envision that our work will lead to research in the following areas. First, through DNA self-assembly technologies (28–30) and other biotechnologies such as enzymatic cleavage (31), metal chelation (31), peptide design, and DNA binding fluorescent conjugated polymers (27), various types of biostructures [such as Holliday junctions (28), 2D or 3D supermolecular structures (28–30), and DNA packing motors (32); see Fig. S8 for some examples] can be employed to provide great flexibility in designing optofluidic lasers as well as other bioinspired optofluidic devices such as biocontrolled photonic switches. Second, instead of using the optical excitation external to the laser system and nonbiological donors (such as dyes), it certainly is possible to develop biooptofluidic lasers that rely on biomolecules such as green fluorescent protein and luciferase to harvest bio- or chemical energy through highly efficient bioluminescence resonance energy transfer (BRET) processes (33). Third, FRET is a widely used technology in biology and chemistry (31, 34). Combination of FRET with highly nonlinear optofluidic lasers can be exploited for highly sensitive intracavity biological and chemical detection (35, 36), which may not be achievable in the linear fluorescence-based detection. Finally, our system may provide a model system for fundamental physics such as lasers at the level of a single molecule or a few molecules.

Materials and Methods

Fabrication of the OFRR Capillary. The details of OFRR fabrication have been previously reported (9, 15). Briefly, a fused silica capillary preform (Polymicro Technologies TSP700850) is first etched with diluted hydrofluoric acid and then rapidly stretched under CO_2 laser irradiation. The resulting OFRR capillary is slightly bulged with a diameter of 75 μm at the center and of a few microns smaller at the two necking points approximately 1 mm apart. This bottle-like structure provides the optical confinement along the OFRR capillary longitudinal direction (37–40). The wall thickness of the OFRR is 3–4 μm (9). The Q factor is approximately 10^7 (9).

Experimental Setup. The experimental setup is illustrated in Fig. S9. A pulsed laser (Continuum Surelite optical parametric oscillator laser, approximately 5-ns pulse width, 20-Hz repetition rate) is loosely focused through a cylindrical lens to excite a 1-mm portion of the OFRR capillary. The pump laser power is adjusted by a neutral density filter. The dye emission is collected in free space through a multimode fiber and then sent to a spectrometer (Triax 550i, Horiba Jobin Yvon, spectral resolution = 0.12 nm).

DNA Preparation. ssDNA samples labeled with dyes are purchased from Integrated DNA Technology (see Tables S1, S2, and Fig. S1 for details). All the DNA sequences are designed using mfold software to minimize possible secondary structure formation (41). The DNA samples are first dissolved in hybridization buffer (PerfectHyb™ Plus, Sigma-Aldrich) to a concentration of 90 μM and then diluted to the desired concentration with Tris acetate-EDTA buffer (pH = 8.3) (Sigma-Aldrich). DNA hybridization is carried out by heating the samples to 45 °C for 3 min, followed by 20 min of cooling at room temperature. Finally, the hybridized sample is flowed through the OFRR with a peristaltic pump at a flow rate of 5 μL/min.

ACKNOWLEDGMENTS. We acknowledge support from the National Science Foundation (CBET-0747398 and ECCS-0853399).

1. Monat C, Domachuk P, Eggleton BJ (2007) Integrated optofluidics: A new river of light. *Nat Photonics* 1:106–114.
2. Li Z, Psaltis D (2007) Optofluidic dye lasers. *Microfluid Nanofluid* 4:145–158.
3. Psaltis D, Quake SR, Yang C (2006) Developing optofluidic technology through the fusion of microfluidics and optics. *Nature* 442:381–386.
4. Qian S-X, Snow JB, Tzeng H-M, Chang RK (1986) Lasing droplets: Highlighting the liquid-air interface by laser emission. *Science* 231:486–488.
5. Tang SKY, et al. (2009) A multi-color fast-switching microfluidic droplet dye laser. *Lab Chip* 9:2767–2771.
6. An K, Moon H-J (2003) Laser oscillations with pumping-independent ultrahigh cavity quality factors in evanescent-wave-coupled-gain microsphere dye lasers. *J Phys Soc Jpn* 72:773–776.
7. Moon H-J, Chough Y-T, An K (2000) Cylindrical microcavity laser based on the evanescent-wave-coupled gain. *Phys Rev Lett* 85:3161–3164.
8. Knight JC, Driver HST, Hutcheon RJ, Robertson GN (1992) Core-resonance capillary-fiber whispering-gallery-mode laser. *Opt Lett* 17:1280–1282.
9. Shopova SI, Zhu H, Fan X, Zhang P (2007) Optofluidic ring resonator based dye laser. *Appl Phys Lett* 90:221101.
10. Jiang X, Song Q, Xu L, Fu J, Tonga L (2007) Microfiber knot dye laser based on the evanescent-wave-coupled gain. *Appl Phys Lett* 90:233501.
11. Helbo B, Kristensen A, Menon A (2003) A micro-cavity fluidic dye laser. *J Micromech Microeng* 13:307–311.
12. Kou Q, Yesilyurt I, Chen Y (2006) Collinear dual-color laser emission from a microfluidic dye laser. *Appl Phys Lett* 88:091101.
13. Balslev S, Kristensen A (2005) Microfluidic single-mode laser using high-order Bragg grating and antiguiding segments. *Opt Express* 13:344–351.
14. Berggren M, Dodabalapur A, Slusher RE, Bao Z (1997) Light amplification in organic thin films using cascade energy transfer. *Nature* 389:466–469.
15. Shopova SI, et al. (2007) Opto-fluidic ring resonator lasers based on highly efficient resonant energy transfer. *Opt Express* 15:12735–12742.
16. Förster T (1959) Transfer mechanism of electronic excitation. *Discuss Faraday Soc* 27:7–17.
17. Armstrong RL, Xie JG, Ruekgauer TE, Pinnick RG (1992) Energy-transfer-assisted lasing from microdroplets seeded with fluorescent sol. *Opt Lett* 17:943–945.
18. Arnold S, Folan LM (1989) Energy transfer and the photon lifetime within an aerosol particle. *Opt Lett* 14:387–389.
19. Leung PT, Young K (1988) Theory of enhanced energy transfer in an aerosol particle. *J Chem Phys* 89:2894–2899.
20. Gotzinger S, et al. (2006) Controlled photon transfer between two individual nanoemitters via shared high-Q modes of a microsphere resonator. *Nano Lett* 6:1151–1154.
21. Clegg RM, Murchie AIH, Zechel A, Lilley DMJ (1993) Observing the helical geometry of double-stranded DNA in solution by fluorescence resonance energy transfer. *Proc Natl Acad Sci USA* 90:2994–2998.
22. Hohng S, Joo C, Ha T (2004) Single-molecule three-color FRET. *Biophys J* 87:1328–1337.
23. Jares-Erijman EA, Jovin TM (1996) Determination of DNA helical handedness by fluorescence resonance energy transfer. *J Mol Biol* 257:597–617.
24. Kukolka F, et al. (2006) A single-molecule Förster resonance energy transfer analysis of fluorescent DNA-protein conjugates for nanobiotechnology. *Small* 2:1083–1089.
25. Lewis FD, Zhang L, Zuo X (2005) Orientation control of fluorescence resonance energy transfer using DNA as a helical scaffold. *J Am Chem Soc* 127:10002–10003.
26. Ali MA, Panoutsopoulos B, Ahmed SA (1992) Potential and limitations of energy-transfer processes in pulsed and cw dye laser mixtures: Comparison of theory and experiments. *Appl Opt* 31:7100–7107.
27. Pun C-C, Lee K, Kim H-J, Kim J (2006) Signal amplifying conjugated polymer-based solid-state DNA sensors. *Macromolecules* 39:7461–7463.
28. Seeman NC (2003) DNA in a material world. *Nature* 421:427–431.
29. Bath J, Turberfield AJ (2007) DNA nanomachines. *Nat Nanotechnol* 2:275–284.
30. Goodman RP, et al. (2008) Reconfigurable, braced, three dimensional DNA nanostructures. *Nat Nanotechnol* 3:93–96.
31. Liu J, Lu Y (2002) FRET study of a trifluorophore-labeled DNAzyme. *J Am Chem Soc* 124:15208–15216.
32. Shu D, Moll W-D, Deng Z, Mao C, Guo P (2004) Bottom-up assembly of RNA arrays and superstructures as potential parts in nanotechnology. *Nano Lett* 4:1717–1723.
33. Xu Y, Piston DW, Johnson CH (1999) A bioluminescence resonance energy transfer (BRET) system: Application to interacting circadian clock proteins. *Proc Natl Acad Sci USA* 96:151–156.
34. Wang K, et al. (2008) Molecular engineering of DNA: Molecular beacons. *Angew Chem Int Edit* 47:2–17.
35. Rose A, Zhu Z, Madigan CF, Swager TM, Bulovi V (2005) Sensitivity gains in chemosensing by lasing action in organic polymers. *Nature* 434:876–879.
36. Wun AW, Snee PT, Chan Y, Bawendi MG, Nocera DG (2005) Non-linear transduction strategies for chemo/biosensing on small length scales. *J Mater Chem* 15:2697–2706.
37. Sumetsky M (2004) Whispering-gallery-bottle microcavities: The three-dimensional etalon. *Opt Lett* 29:8–10.
38. Louyer Y, Meschede D, Rauschenbeute A (2005) Tunable whispering-gallery-mode resonators for cavity quantum electrodynamics. *Phys Rev A* 72:031801(R).
39. Pöllinger M, O'Shea D, Warken F, Rauschenbeutel A (2009) Ultrahigh-Q tunable whispering-gallery-mode microresonator. *Phys Rev Lett* 103:053901.
40. Murugan GS, Wilkinson JS, Zervas MN (2009) Selective excitation of whispering gallery modes in a novel bottle microresonator. *Opt Express* 17:11916–11925.
41. Zuker M (2003) Mfold web server for nucleic acid folding and hybridization prediction. *Nucl Acids Res* 31:3406–3415.